The Thesis Committee for Emily Janette Powell
Certifies that this is the approved version of the following thesis:

A Lithium Conducting Phase (Li_2Te) Can Obviate Need for Nanocrystallites in the Lithiation/De-lithiation of Germanium

APPROVED BY
SUPERVISING COMMITTEE:

Supervisor:

C. Buddie Mullins

Adam Heller

A Lithium Conducting Phase (Li_2Te) Can Obviate Need for Nanocrystallites in the Lithiation/De-lithiation of Germanium

by

Emily Janette Powell, B.S.

Thesis

Presented to the Faculty of the Graduate School of

The University of Texas at Austin

in Partial Fulfillment

of the Requirements

for the Degree of

Master of Arts

The University of Texas at Austin

August 2015

Dedication

I would like to dedicate this thesis to my parents, sister, and friends for always supporting me.

Acknowledgements

I would like to thank my friends and family for supporting me in this endeavor. I would also like to thank my advisor Dr. Buddie Mullins and co-advisor Dr. Adam Heller for their advice and support. Fellow group members Sean Wood, Hoang Dang, and Paul Abel also provided immense amounts of information and support.

Abstract

A Lithium Conducting Phase (Li_2Te) Can Obviate Need for Nanocrystallites in the Lithiation/De-lithiation of Germanium

Emily Janette Powell, M.A.

The University of Texas at Austin, 2015

Supervisor: C. Buddie Mullins

Mainstream rechargeable lithium battery materials research of the past 20 years has focused on nano-particulate materials, where Li^+-diffusion lengths exceeded at designated cycling rates the particle radii, and where the particles slipped rather than broke upon their expansion and shrinkage in lithiation/de-lithiation cycles. Here we show that in intrinsically rapidly Li^+-transporting macrocrystalline germanium and even more so in a dispersion of non-cycling Li_2Te in macrocrystalline germanium it is unnecessary to use nanocrystalline materials and that Li_2Te increases the retained capacity at 1C rate after 500 cycles. Dispersions of 10-30 atom % of crystalline GeTe in 90-70 atom % crystalline Ge were synthesized by quenching from the melt followed by high energy ball milling to 1μm-5μm particle size. The particles, as well as similarly made and similarly sized pure Ge particles were incorporated in electrodes, which were galvanostatically lithiated/de-lithiated. In the initial cycle, GeTe is reduced to Li_xGe alloys and Li_2Te. In 500 1C cycles of Li_xGe de-lithiation/Ge lithiation the capacity of the pure Ge faded more

rapidly than that of the Ge electrodes containing Li_2Te, which retained 94-96 % of their initial capacity after 500 cycles at 1C rate.

Table of Contents

List of Tables

List of Figures

Chapter 1: A Lithium Conducting Phase (Li_2Te) Can Obviate Need for Nanocrystallites in the Lithiation/De-lithiation of Germanium[1]

INTRODUCTION

About 5,000 papers describe improvements through use of nanoparticles instead of larger particle lithiated/de-lithiated electrode materials. Because diffusivities decrease in the order solution > surface > grain boundary > lattice-defects > perfect lattice[1-4], the large specific surface of nanoparticles provides for rapid cycling. Use of nanoparticles also reduces mechanical failure, as small particles and grains slip before breaking under the stress associated with the expansion/shrinkage upon lithiation/de-lithiation.[5] Here we present an example where cycling efficiency and stability are sustained in macroparticles by a dispersed non-cycling lithium-conducting phase.

Germanium is one of the faster Li^+ transporters.[6, 7] Were it not for its high cost, it would be a candidate anode material in lithium ion batteries.[8] The diffusivity of lithium in crystalline germanium is at $6.25x10^{-12}$ cm^2 s^{-1} two orders of magnitude faster than in silicon, and its theoretical specific capacity upon cycling between Ge and $Li_{15}Ge_4$, a stable alloy at ambient temperature[9], is 1,383 mA h g^{-1}.[6, 10, 11] Because the volume of $Li_{15}Ge_4$ is greater than 3 times that of Ge, the volume change breaks larger Ge crystals causing capacity fade.[12] However, small crystallites slip under stress before they fail, and capacity fading is reduced in pure and chalcogenide containing nano-structured Ge[6, 13-15,16-18] including $Ge_{0.95}S_{0.05}$ and $Ge_{0.90}Se_{0.10}$.[19-21] The cycling of SnSe[22] and PbTe, where Li^+-conducting Li_2Te is co-produced with the Li_xPb alloys, are also stable.[23] Studies using C and Te composites have also been performed.[24, 25] Here we extend the studies to $Ge_{0.95}Te_{0.05}$, $Ge_{0.90}Te_{0.10}$, and $Ge_{0.85}Te_{0.15}$, Ge-GeTe composites, which are lithiated to

[1] Portions of this chapter have been previously published: Emily J. Powell, et. al. "Obviating the need for nanocrystallites in the extended lithiation/de-lithiation of germanium" 2015. *Submitted*.

$Li_{15}Ge_4$ and Li_2Te. We find that the Li_2Te associated defects in the formed alloy, possibly $Li_{15}Ge_4$, are beneficial, preventing capacity fade.

EXPERIMENTAL

Materials synthesis and characterization

Pure tellurium (Acros Organics, 99.8% 200 mesh) and germanium (Kurt Lesker, 99.999%) were combined in sub-stoichiometric amounts in a quartz ampule. The quartz ampule was evacuated to a pressure of 1 x 10^{-5} torr and sealed. The ampule was heated in a tube furnace (Thermo Scientific Lindberg Blue M) with constant rotation to a temperature of 990 °C at a rate of 5 °C/min and then heated to 1000 °C at a rate of 0.5 °C/min. The ampule was held at 1000 °C for 36 h followed by quenching in ice water. This synthesis was adapted from Chakraborty's sub-sulfide work.[26] The material was extracted from the ampule in an argon-filled glove-box (MBraun Unilab) with oxygen and water levels held below 5 ppm, and ball milled under argon for 48 h at 450 rpm with 5 minutes on followed by 5 minutes off. 3mm ZrO_2 balls were used in a mass ratio of 40:1 with the Ge or $Ge_{(1-x)}Te_x$ materials. The ball-milled materials were stored in the glove-box.

Scanning Electron Microscopy (SEM) micrographs were obtained using a Hitachi S-5500 electron microscope. Energy Dispersion X-ray Spectroscopy (EDX) spectra were obtained with a Bruker detector on the same instrument.

X-ray Diffraction (XRD) measurements were performed on a Rigaku MiniFlex 600 diffractometer with a Cu Kα radiation source at 40kV and 15mA. MDI JADE[27] software was used for peak identification and fitting and Williamson-Hall plot analysis. The standard to determine instrumental broadening was LaB_6. A pseudo-Voight fit with linear background was used. The Lorentzian contribution was 0.5 and the skewness was

0.0. The initial width used was full width half max (FWHM) and there were peaks present for K2α radiation. The R value, to evaluate a good fit of the model, was less than 10% for all materials. A value of less than 10% indicates a good fit.

Electrochemical measurements

An aqueous slurry of Ge, $Ge_{0.95}Te_{0.05}$, $Ge_{0.90}Te_{0.10}$, or $Ge_{0.85}Te_{0.15}$ particles (60 wt%), 90 kDa carboxymethyl cellulose (20 wt%) binder, and Super P Li^+-conductive carbon (Timcal, 20 wt%) was slurry cast onto copper foil and dried in a vacuum oven at 120 °C for 12 h. This film was punched into disks that formed the working electrodes of CR 2032 coin-type cells. Each electrode had a mass loading of 340-370 μg cm^{-2}. The cells were assembled in an argon-filled glovebox with lithium foil (Alfa Aesar 99%) as the counter and reference electrodes and Celgard 2400 polypropylene membrane as the separator. A solution of 1M $LiPF_6$ (Sigma Aldrich, battery grade) in 1:1 v/v fluoroethylene carbonate (Solvay Fluor) and diethyl carbonate (Sigma Aldrich, battery grade) was used as the electrolyte. Electrochemical measurements were performed on an Arbin BT2043 or BT2143 multichannel battery testing system. Cells were cycled between 5 mV and 1.25 V versus Li/Li^+.

RESULTS AND DISCUSSION

Use of melt-quench synthesis techniques allows access to thermodynamically unstable phases with good mixing because all materials are in a liquid or gas phase during synthesis.[28] Upon quenching, GeTe is the only stable phase that can form and excess Ge is expected to crystallize out of the melt.[29]

The XRD plots in Figure 1 compare micrometer-sized particles of Ge, $Ge_{0.95}Te_{0.05}$, $Ge_{0.90}Te_{0.10}$, and $Ge_{0.85}Te_{0.15}$. The presence of peaks in the XRD spectra indicates that the materials are relatively crystalline. The peak broadness is attributed to

small crystallite size which is a function of the high-intensity ball milling procedure. The peaks in Ge are exclusively assigned to the Ge reflections in the reference material, Figure 1(b). As the percentage of tellurium increases, a peak around $2\theta = 30°$ begins to appear that corresponds to the GeTe phase. The majority of the peaks in $Ge_{0.90}Te_{0.10}$ and $Ge_{0.85}Te_{0.15}$ are assigned to the reflections in the Ge reference, with an additional peak at about $2\theta = 30°$ that indicates the presence of the GeTe phase. In the $Ge_{0.95}Te_{0.05}$ material there is not enough tellurium present to visualize a peak at $2\theta = 30°$. However, EDX (Figure 4) indicates there is Te present, which is assumed to be in the GeTe phase. The XRD spectra indicate that the $Ge_{(1-x)}Te_x$ materials are composed of two phases: a Ge phase and a GeTe phase.

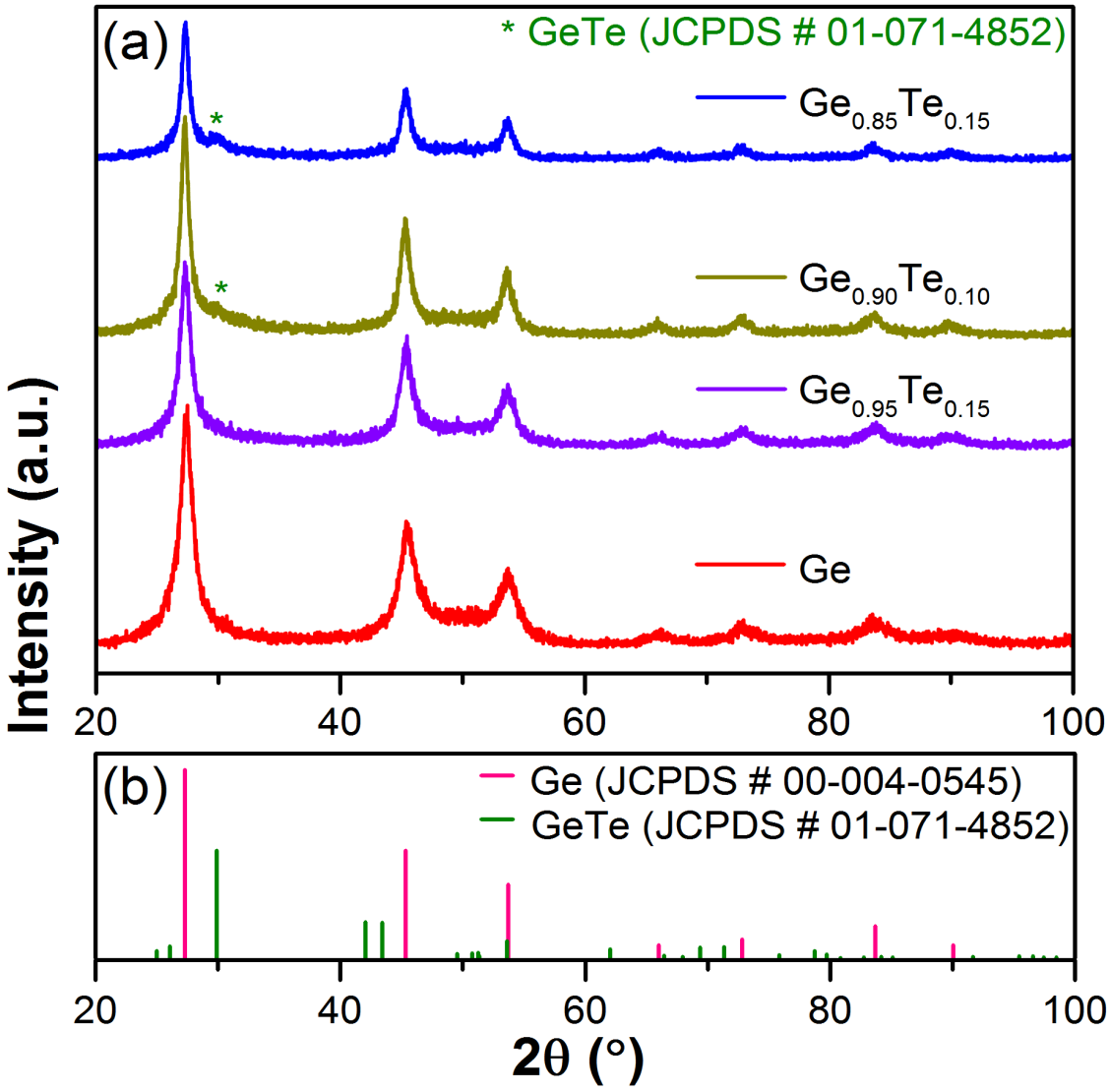

Figure 1. XRD of (a) micrometer-sized Ge, $Ge_{0.95}Te_{0.15}$, $Ge_{0.90}Te_{0.10}$, and $Ge_{0.85}Te_{0.15}$; (b) reference reflections of Ge and GeTe.

A Williamson-Hall plot was created for each material to determine crystallite size. The width of the peaks in the XRD plots are a function of three parameters: crystallite size, crystallite strain, and instrumental broadening. The instrumental broadening was taken into account by running a standard of LaB_6. With this standard, any peak broadening is attributed to the instrument and is subtracted from experimental $Ge_{(1-x)}Te_x$

samples. Crystallite size and strain are analyzed using a Williamson-Hall plot. The slope of the line in the Williamson-Hall plot gives information about the strain of the material. Table 1, below, shows the calculated crystallite sizes for the Ge and $Ge_{(1-x)}Te_x$ materials.

Material	Atomic % Ge	Atomic % Te	Crystallite size (nm)	Strain (%)
Germanium	100	0	7.4(0.4)	0.387
$Ge_{0.95}Te_{0.05}$	96	4	11.2(0.9)	0.443
$Ge_{0.90}Te_{0.10}$	92	8	14.6(1.7)	0.329
$Ge_{0.85}Te_{0.15}$	88	12	20.6(2.6)	0.453

Table 1. Crystallite size and strain for germanium, $Ge_{0.95}Te_{0.05}$, $Ge_{0.90}Te_{0.10}$, and $Ge_{0.85}Te_{0.15}$ as determined from XRD. Standard deviation in crystallite size is given in parentheses after the crystallite size value. Atomic percent composition of germanium and tellurium was determined by EDX.

The crystallite size increases as the percentage of tellurium increases. This is contrary to what was expected. As tellurium was added, it was expected that the material would become more brittle and this would increase the number of grain boundaries and decrease the crystallite size. However, the tellurium seems to increase the crystallite size, though a 20.6nm crystallite is still very small.

XRD spectra of Ge and $Ge_{0.85}Te_{0.15}$ were also measured after at least 500 cycles at 1C rate (Figure 2). The electrodes were de-lithiated to 1.25V vs. Li/Li^+ or lithiated to 10mV vs. Li/Li^+ and were scanned from 25° to 30°. The cycled $Ge_{0.85}Te_{0.15}$ electrode shows, when lithiated, a peak at 26.2°, attributed to $Li_{15}Ge_4$, PDF #01-089-2584. The XRD spectrum of the $Ge_{0.85}Te_{0.15}$ electrode, but not in the Ge electrode, also shows both when lithiated and de-lithiated a very broad low intensity reflection at 27.6° which is attributed to non-cycling germanium. After cycling, the XRD spectrum of the Ge electrode (Figure 2) does not show its initial reflection (Figure 1) or any other reflection,

suggesting that cycling made it amorphous. In the de-lithiated $Ge_{0.85}Te_{0.15}$ electrode the broad and weak 27.6° germanium reflection is observed both in the lithiated and de-lithiated electrodes after more than 500 cycles, suggesting that not all of the Ge is cycling and that the non-cycling Ge is crystalline. Most of the Ge of the $Ge_{0.85}Te_{0.15}$ electrode is, however, amorphous and cycling.

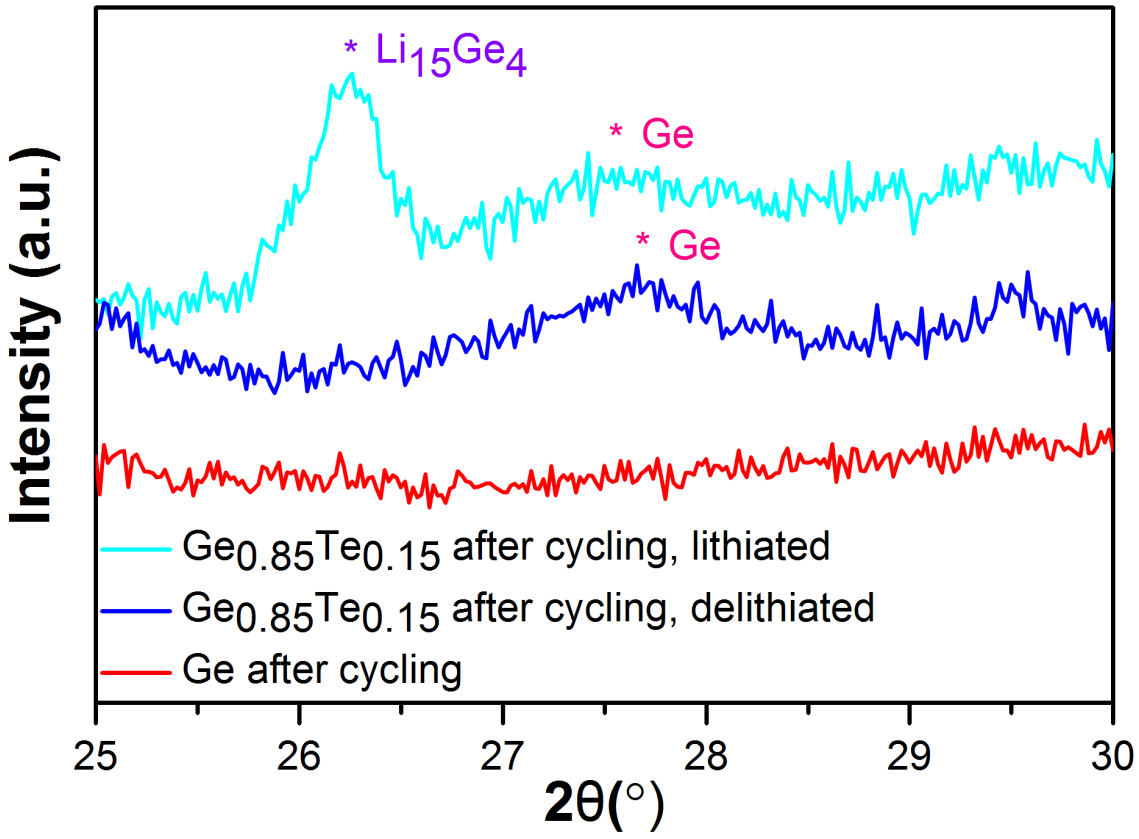

Figure 2. XRD of $Ge_{0.85}Te_{0.15}$ and Ge electrodes after more than 500 cycles at a rate of 1C.

The particle size of the germanium and germanium sub-telluride materials was examined using SEM. According to multiple SEM images taken of each material, the average particle size was 3μm and the particles ranged in size from 1μm to 5μm.

Occasionally a particle larger than 10μm was seen, but they were very rare. The SEM images in Figure 3 show micrometer-sized particles of germanium, $Ge_{0.95}Te_{0.05}$, $Ge_{0.90}Te_{0.10}$, and $Ge_{0.85}Te_{0.15}$ with small fines agglomerating to the surface, this is a typical feature of making particles using high-intensity ball-milling. The majority of the mass of the material is in the micrometer-sized particles, and they are the only particles considered when discussing particle size.

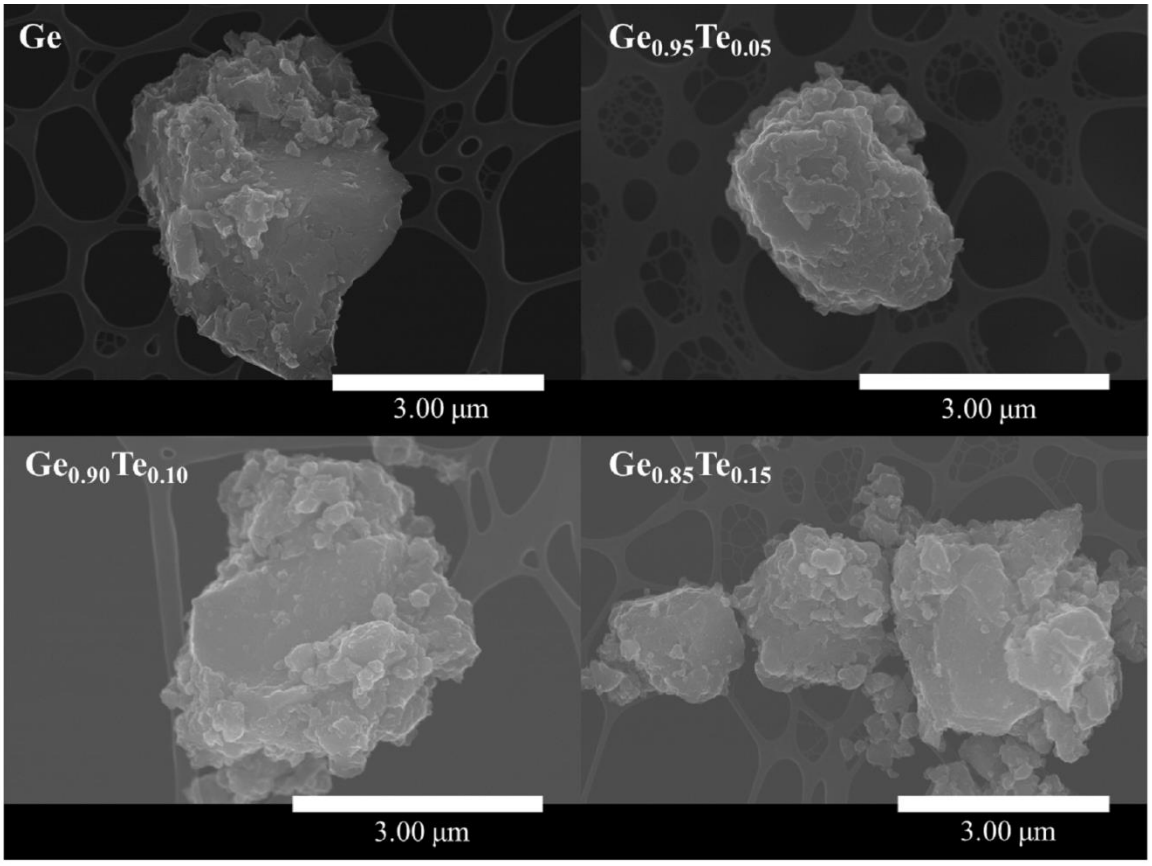

Figure 3. SEM images of Ge, $Ge_{0.95}Te_{0.05}$, $Ge_{0.90}Te_{0.10}$, $Ge_{0.85}Te_{0.15}$.

Energy dispersive x-ray spectroscopy (EDX) is a method used to characterize what elements are present and how they are distributed in a given material. EDX color mapping images, Figure 4, indicate that germanium and tellurium are homogeneously distributed across individual particles. In Figure 4 the red dots correspond to Ge and green dots correspond to Te. The location of the dots indicates the two elements are evenly distributed across the particle. The tellurium is present as GeTe, and the even distribution of the green dots on the images in Figure 4 suggest that there are no isolated domains of GeTe. In other words, GeTe is spread uniformly across the entire particle.

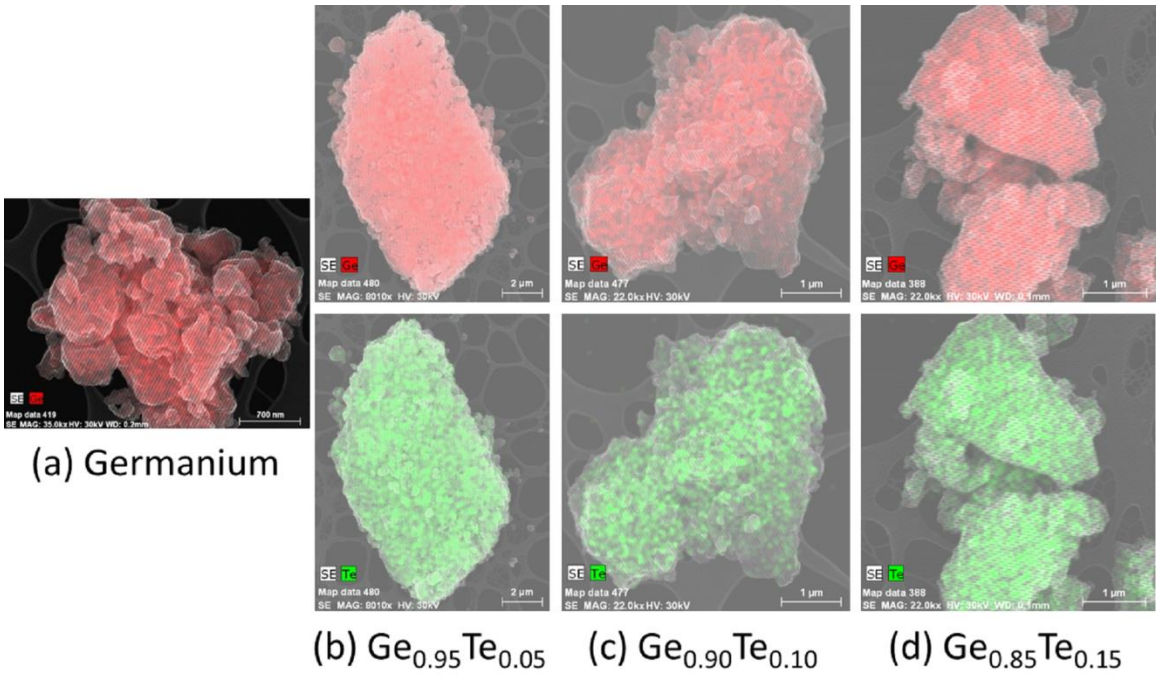

Figure 4. EDX color mapping of (a) pure Ge, (b) $Ge_{0.95}Te_{0.05}$, (c) $Ge_{0.90}Te_{0.10}$, and (d) $Ge_{0.85}Te_{0.15}$. The red color represents germanium atoms and the green color represents tellurium atoms.

EDX was also used to determine the actual atomic composition of germanium and tellurium in the synthesized materials. The results of multiple EDX scans were averaged

and the percent atomic composition values are shown in Table 2. The values in Table 2 indicate that some tellurium was lost during the synthesis steps, and the atomic percentage of germanium is slightly higher than expected. These experimental values of elemental atomic percent composition were taken into account when calculating the theoretical capacity, but the materials will continue to be referred to with their theoretical composition names.

Material	**Atomic Composition Germanium (%)**	**Error (%)**	**Atomic Composition Tellurium (%)**	**Error (%)**
Ge	100	0	0	0
$Ge_{0.95}Te_{0.05}$	96	6	4	0.6
$Ge_{0.90}Te_{0.10}$	92	7	8	1
$Ge_{0.85}Te_{0.15}$	88	5	12	2

Table 2. Atomic compositions of the as-synthesized Ge, $Ge_{0.95}Te_{0.05}$, $Ge_{0.90}Te_{0.10}$, $Ge_{0.85}Te_{0.15}$ materials.

Another EDX function to determine the spread of different elements across individual particles is an EDX line scan. A representative line scan across a particle of each $Ge_{(1-x)}Te_x$ alloy is shown in Figure 5(a)-(c). A line scan moves step-wise across a particle in the direction and speed set by the user in the EDX software. At each step the instrument analyzes what elements are present and in what ratios. In Figure 5, the red line corresponds to germanium and the green line corresponds to tellurium. In the line scans below, the constant ratio of Ge and Te signal suggests that the two elements are

uniformly distributed across the length of each particle. This confirms the elemental distribution seen by EDX color mapping in Figure 4. These lines scans and EDX color images are representative of what was seen in every particle examined.

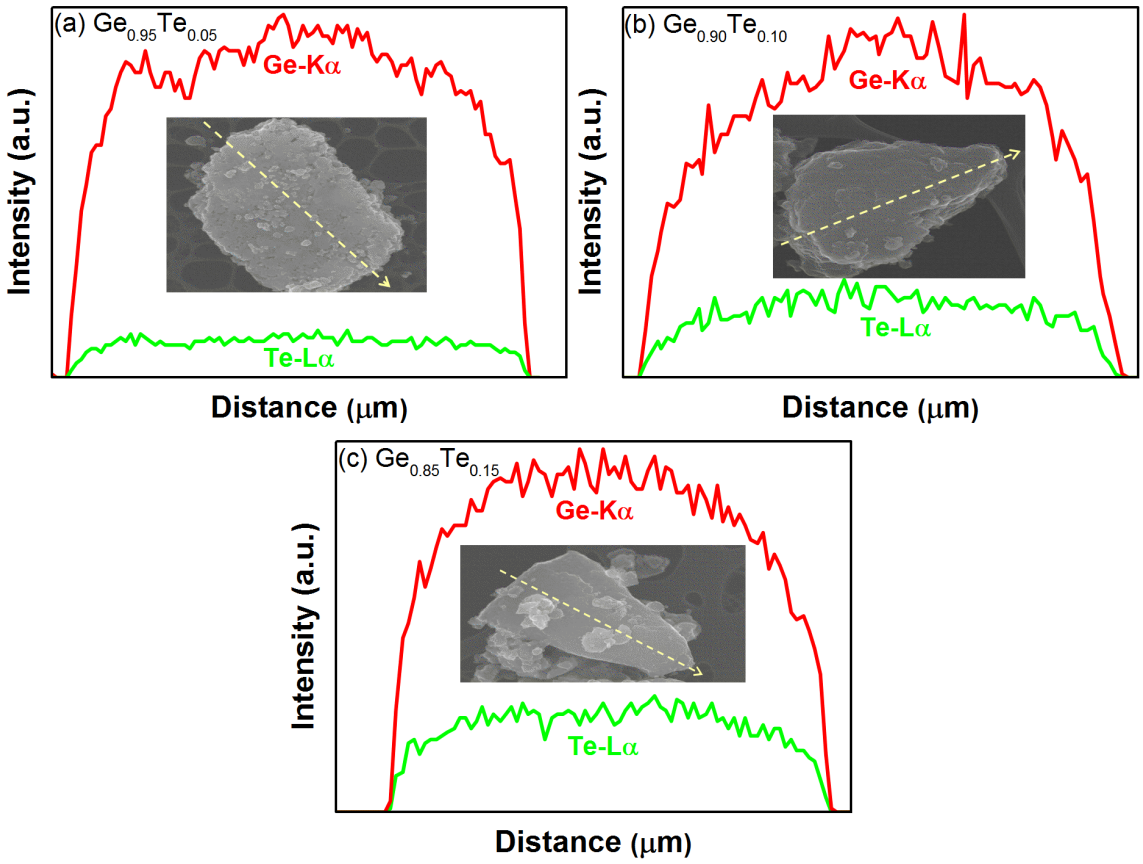

Figure 5. Representative EDX line scans across (a) $Ge_{0.95}Te_{0.05}$, (b) $Ge_{0.90}Te_{0.10}$, (c) $Ge_{0.85}Te_{0.15}$ particles. The SEM image of the scanned particle is inset into the line scan plots. Red represents germanium and green represents tellurium.

After the first lithiation, the germanium sub-telluride electrodes become Ge-Li_2Te materials. Figure 6 shows a cyclic voltammogram of the $Ge_{(1-x)}Te_x$ materials at cycle 3. Cycle 3 was chosen because it provides enough time for all reactions to occur and come to equilibrium. In $Ge_{0.85}Te_{0.15}$ and $Ge_{0.90}Te_{0.10}$ a Li_2Te peak at 1.75 V vs. Li/Li^+ is

observed; it is attributed to the formation of Li_2Te [30], its Gibbs free energy of formation providing 1.78 V. The peaks below 0.75V vs. Li/Li^+ in Figure 6(a)-(d) correspond to the formation of Li-Ge alloys.[10, 31]

The cyclic voltammograms indicate that Li_2Te forms when the material is at a voltage at which Te will react. During cycling the Li_2Te phase is only formed during the first cycle. The cell starts at open circuit potential which averages around 3.0 V vs. Li/Li^+. As current is applied, the voltage decreases and Li^+ is inserted into the material. Around a potential of 1.78 V vs. Li/Li^+ the reaction of Li^+ with Te occurs. During cycling, this is an irreversible reaction because the cell will never again go through that potential range. For cycling, the cells oscillate through a 5mV to 1.25 V vs. Li/Li^+ voltage window, germanium, though not tellurium, reacts in this range. The reaction of Li^+ with Te results in an irreversible capacity loss, however it forms a Li_2Te phase which has two purposes: conduct Li^+ and incorporate more grain boundaries into the Ge material, both facilitate increased charge transfer.

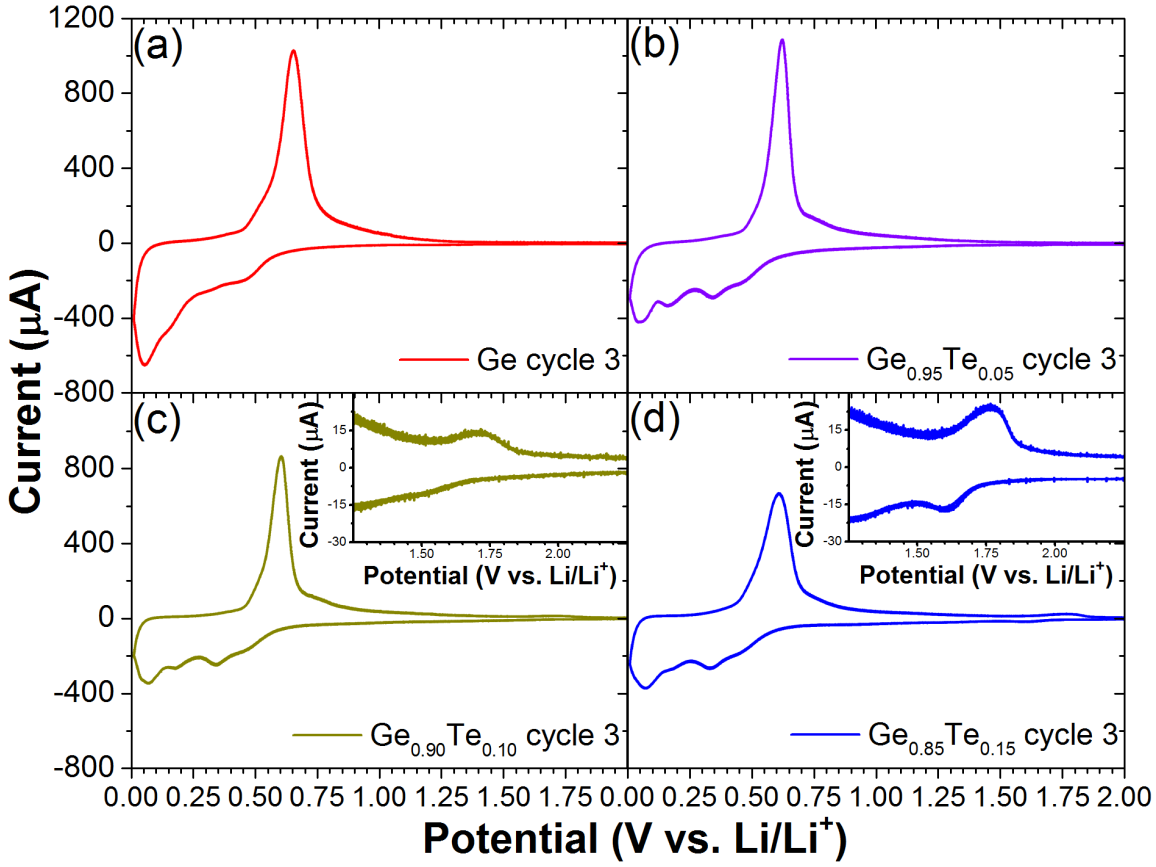

Figure 6. Cyclic voltammetry plots for (a) Ge, (b) $Ge_{0.95}Te_{0.05}$, (c) $Ge_{0.90}Te_{0.10}$, (d) $Ge_{0.85}Te_{0.15}$.

The $Ge_{(1-x)}Te_x$ electrodes underwent a C-rate test, Figure 7, that examined their ability to cycle at high rates of charge and discharge for short periods of time. The test started with a charging cycle at a rate of C/20. A rate of C/20 indicates that one charge cycle is completed in 20 hours and one discharge cycle is completed in 20 hours. The conditioning cycle was followed by 5 cycles each of the following rates: C/10, C/5, C/2, 1C, 2C, 5C, 10C, 5C, 1C, C/2, and C/5. After cycling at a rate of 10C the current applied was decreased to examine how the electrodes would recover from fast cycling. Figure 7(a) shows the specific capacity of Ge (red), $Ge_{0.95}Te_{0.05}$ (purple), $Ge_{0.90}Te_{0.10}$ (green), and $Ge_{0.85}Te_{0.15}$ (blue). As expected, the pure germanium electrode has the highest

capacity because it is composed of 100% active material. The capacities decrease in the order Ge > $Ge_{0.90}Te_{0.10}$ > $Ge_{0.85}Te_{0.15}$ > $Ge_{0.95}Te_{0.05}$. It is unknown why $Ge_{0.95}Te_{0.05}$ cycles at such a low capacity, though it is composed of 95% active material. After 5 cycles at 10C and returning to 1C, the $Ge_{0.85}Te_{0.15}$ electrode exceeds the capacity of the first 5 cycles at 1C.

Figure 7(b) shows the capacity retention of the electrodes in the C-rate test. The capacity retention at high C-rates is relatively low, however at slower C-rates most of the electrode materials retain between 90-100% of their capacity. Capacity retention was determined by dividing the capacity of a given cycle by the highest capacity seen in the first five cycles at C/10 and multiplying by 100%. For $Ge_{0.95}Te_{0.05}$ the electrode starts to rapidly fade at a 2C C-rate, while the other electrodes do not drastically fade until a C-rate of 5C is applied. In the second set of 1C cycles the electrodes do recover the capacity retention they had in the initial 1C cycle, after cycling at 10C.

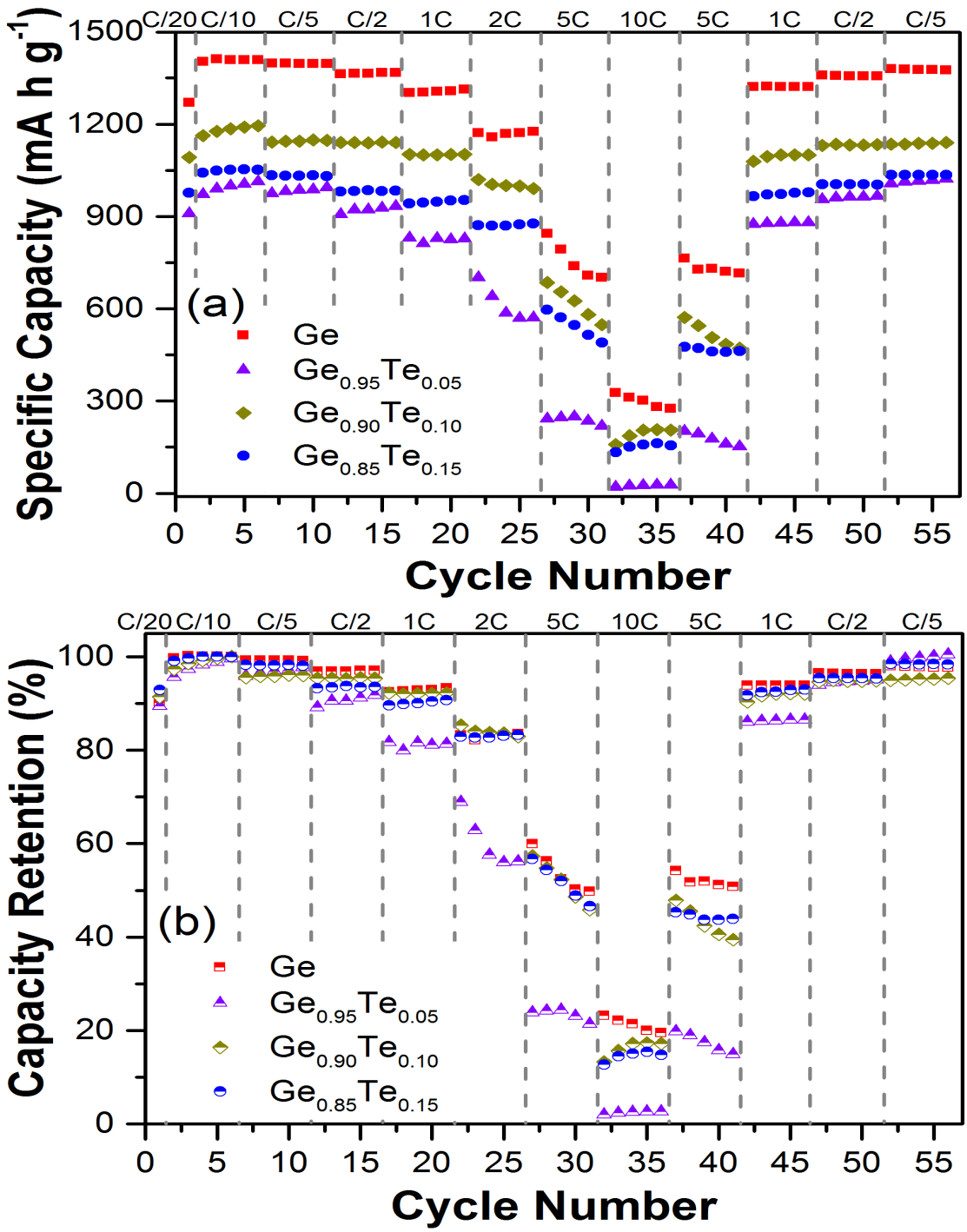

Figure 7. (a) Specific capacity and (b) capacity retention of Ge (red), $Ge_{0.95}Te_{0.05}$ (purple), $Ge_{0.90}Te_{0.10}$ (green), $Ge_{0.85}Te_{0.15}$ (blue) at varying C-rates.

The $Ge_{(1-x)}Te_x$ electrodes were cycled at a rate of C/5 for 100 cycles (Figure 8). Again, the pure germanium electrode has the highest specific capacity because it is composed of 100% active material. In this extended cycling test, the $Ge_{0.95}Te_{0.05}$ and $Ge_{0.90}Te_{0.10}$ electrodes have lower specific capacities than the $Ge_{0.85}Te_{0.15}$ electrode, Figure 8(a). This suggests that the $Ge_{0.85}Te_{0.15}$ is an ideal ratio of Ge and Te, to achieve the highest specific capacity values, after Ge.

Theoretically, the specific capacities of Ge, $Ge_{0.95}Te_{0.05}$, $Ge_{0.90}Te_{0.10}$, and $Ge_{0.85}Te_{0.15}$ are 1383 mA h g^{-1}, 1289 mA h g^{-1}, 1200 mA h g^{-1}, and 1116 mA h g^{-1}, respectively. Experimentally, Ge has the highest specific capacity followed by $Ge_{0.85}Te_{0.15}$, $Ge_{0.95}Te_{0.05}$, and $Ge_{0.90}Te_{0.10}$, Figure 8(a). Ge starts cycling at a rate of C/5 with a specific capacity of 1270 mA h g^{-1}, and this value continues to increase until it achieves 1323 mA h g^{-1} at cycle 100. This constant increase in capacity means that any capacity retention calculated will be greater than 100%, Figure 8(b). We hypothesize that the capacity increases because the germanium particles break-up upon lithiation and continuously expose fresh germanium surfaces to lithiate. The coulombic efficiency averages at 99%, though it does decrease to around 98% in cycles 40-60. Low coulombic efficiency is expected since the particles are micrometer-sized.

$Ge_{0.85}Te_{0.15}$ starts cycling at a rate of C/5 with an initial specific capacity of 1203 mA h g^{-1}. The highest specific capacity occurs at cycle 5, 1218 mA h g^{-1}, and this value is used in calculating capacity retention. After 100 cycles, the $Ge_{0.85}Te_{0.15}$ material has a specific capacity of 1197 mA h g^{-1}, which corresponds to a capacity retention of 98%. The coulombic efficiency of this material averages 99%.

$Ge_{0.95}Te_{0.05}$ starts cycling at a rate of C/5 with an initial specific capacity of 1116 mA h g^{-1}. The highest specific capacity occurs in the conditioning cycle at a rate of C/20, 1171 mA h g^{-1}, and this value is used to calculate capacity retention. After 100 cycles the

specific capacity is 1168 mA h g^{-1}, which corresponds to a capacity retention of 99.8%. The coulombic efficiency of this material averages at 95%.

$Ge_{0.90}Te_{0.01}$ starts cycling at a rate of C/5 with an initial specific capacity of 995 mA h g^{-1}. This value increases over the first 8 cycles until the maximum capacity, 1033 mA h g^{-1}, is achieved at cycle 8. This value is used in calculating capacity retention. After 100 cycles specific capacity is 1045 mA h g_{-1} which corresponds to a capacity retention greater than 100%. This indicates that the capacity of the material slowly increases over the first 100 cycles. The coulombic efficiency averages as 99%.

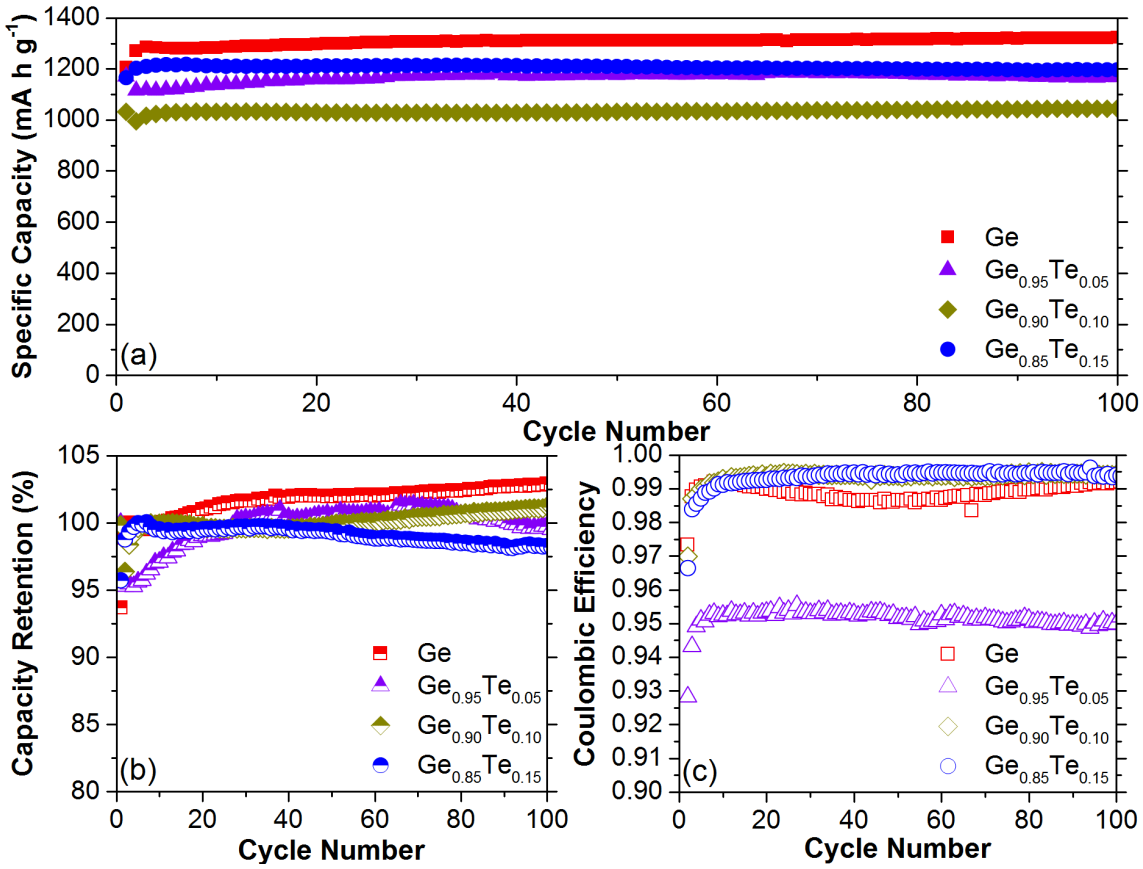

Figure 8. (a) Comparison of Ge (red), $Ge_{0.95}Te_{0.05}$ (purple), $Ge_{0.90}Te_{0.10}$ (green), and $Ge_{0.85}Te_{0.15}$ (blue) lithiation/delithiation capacity dependence at a cycling rate of C/5. Also shown are (b) percent capacity retention and (c) coulombic efficiency, both at a rate of C/5.

Additionally, the $Ge_{(1-x)}Te_x$ electrodes were cycled for 500 cycles at a rate of 1C, Figure 9. The $Ge_{0.85}Te_{0.15}$ electrode was cycled at 1C for 1000 cycles, Figure 10. The 1C cycling results differ between the $Ge_{(1-x)}Te_x$ materials, as shown in Figure 9(a). $Ge_{0.85}Te_{0.15}$ seems to be the optimal composition because it has the highest capacity after Ge and cycles very stably over 500 cycles. Pure Ge has a higher theoretical capacity than $Ge_{0.85}Te_{0.15}$ (1383 mA h g^{-1} and 1116 mA h g^{-1}, respectively), and initially starts at a higher capacity than $Ge_{0.85}Te_{0.15}$ but it quickly fades and around cycle 40 its capacity is lower than that of $Ge_{0.85}Te_{0.15}$. After 500 cycles the Ge electrode has a specific capacity

of 983 mA h g^{-1}. In contrast, $Ge_{0.85}Te_{0.15}$ cycles stably over 500 cycles. After 500 cycles $Ge_{0.85}Te_{0.15}$ has a specific capacity of 1002 mA h g^{-1}. After 500 cycles Ge retains only 82% maximum capacity while $Ge_{0.85}Te_{0.15}$ retains 96% maximum capacity, Figure 9(b). The materials exhibit the opposite trend with coulombic efficiency, Figure 9(c), with Ge averaging 99.7% coulombic efficiency and $Ge_{0.85}Te_{0.15}$ averaging 98.2% coulombic efficiency.

Capacity retention for Ge and $Ge_{0.85}Te_{0.15}$ was calculated by looking at the capacity of a given cycle and dividing it by the highest capacity seen in the first 10 cycles. For $Ge_{0.85}Te_{0.15}$ the highest capacity in the first 10 cycles was the C/20 conditioning cycle at 1045 mA h g^{-1}. This initial capacity was surpassed during cycles 37-249, which resulted in more than 100% capacity retention for those cycles. The highest specific capacity seen was 1057 mA h g^{-1}. This increase in capacity can be attributed to the formation of additional grain boundaries which facilitate the diffusion of lithium during these cycles. The highest capacity of Ge in the first 10 cycles was in cycle 5 at 1193 mA h g^{-1}. This was the highest specific capacity seen in all 500 cycles.

$Ge_{0.95}Te_{0.05}$ and $Ge_{0.90}Te_{0.10}$ cycle stably over 500 cycles but both have a lower experimental specific capacity than $Ge_{0.85}Te_{0.15}$. $Ge_{0.95}Te_{0.05}$ starts cycling at a rate of 1C with a specific capacity of 944 mA h g^{-1}, though this number steadily increases over the first 30 cycles until it stabilizes around 970 mA h g^{-1}. We hypothesize that the specific capacity increases over the first few cycles as the micrometer-sized particles break up and expose more germanium active material. After 500 cycles $Ge_{0.95}Te_{0.05}$ has a specific capacity of 952 mA h g^{-1} and retains 94% of its maximum capacity, Figure 9(b). The maximum capacity, 1015 mA h g^{-1}, was achieved in the C/20 conditioning cycle. The coulombic efficiency averaged at 98%, Figure 9(c), which is not unusual for large micrometer-sized particles.

$Ge_{0.90}Te_{0.10}$ had an initial specific capacity at a rate of 1C of 855 mA h g^{-1}, Figure 9(a). This initial specific capacity increased over the first 30 cycles to a specific capacity of 909 mA h g^{-1}. After 500 cycles $Ge_{0.90}Te_{0.10}$ had a specific capacity of 908 mA h g^{-1} and a capacity retention of 95%, Figure 9(b). The maximum capacity, 949 mA h g^{-1}, was achieved in the conditioning cycle at a rate of C/20. As with the $Ge_{0.95}Te_{0.05}$ material, we hypothesize that the specific capacity increases over the first few cycles as the micrometer-sized particles break up and expose more germanium active material. The coulombic efficiency averaged around 94% and was the lowest coulombic efficiency seen among the four materials, Figure 9(c).

The $Ge_{0.85}Te_{0.15}$ electrode was cycled at a rate of 1C to 1000 cycles, Figure 10. After 1000 cycles $Ge_{0.85}Te_{0.15}$ had a specific capacity of 922 mA h g^{-1}, which corresponds to 88% capacity retention. The Ge, $Ge_{0.95}Te_{0.05}$, $Ge_{0.90}Te_{0.10}$ electrodes all stopped cycling after 500 cycles.

Stability can be visualized by looking at the capacity retention of the $Ge_{(1-x)}Te_x$ materials, Figure 9(b) and 10. After 500 cycles Ge, $Ge_{0.95}Te_{0.05}$, $Ge_{0.90}Te_{0.10}$, and $Ge_{0.85}Te_{0.15}$ retain 82%, 94%, 95%, and 96% of their initial capacity, respectively. After 500 cycles the specific capacity of the $Ge_{0.85}Te_{0.15}$ material begins to fade and after 1000 cycles it retains only 88% of its initial capacity. The capacity retention values for $Ge_{0.95}Te_{0.05}$, $Ge_{0.90}Te_{0.10}$, and $Ge_{0.85}Te_{0.15}$ after 500 cycles are all greater than 90%, and this indicates that the materials cycle stably. All the materials containing Te cycle with more stability than the pure Ge electrode.

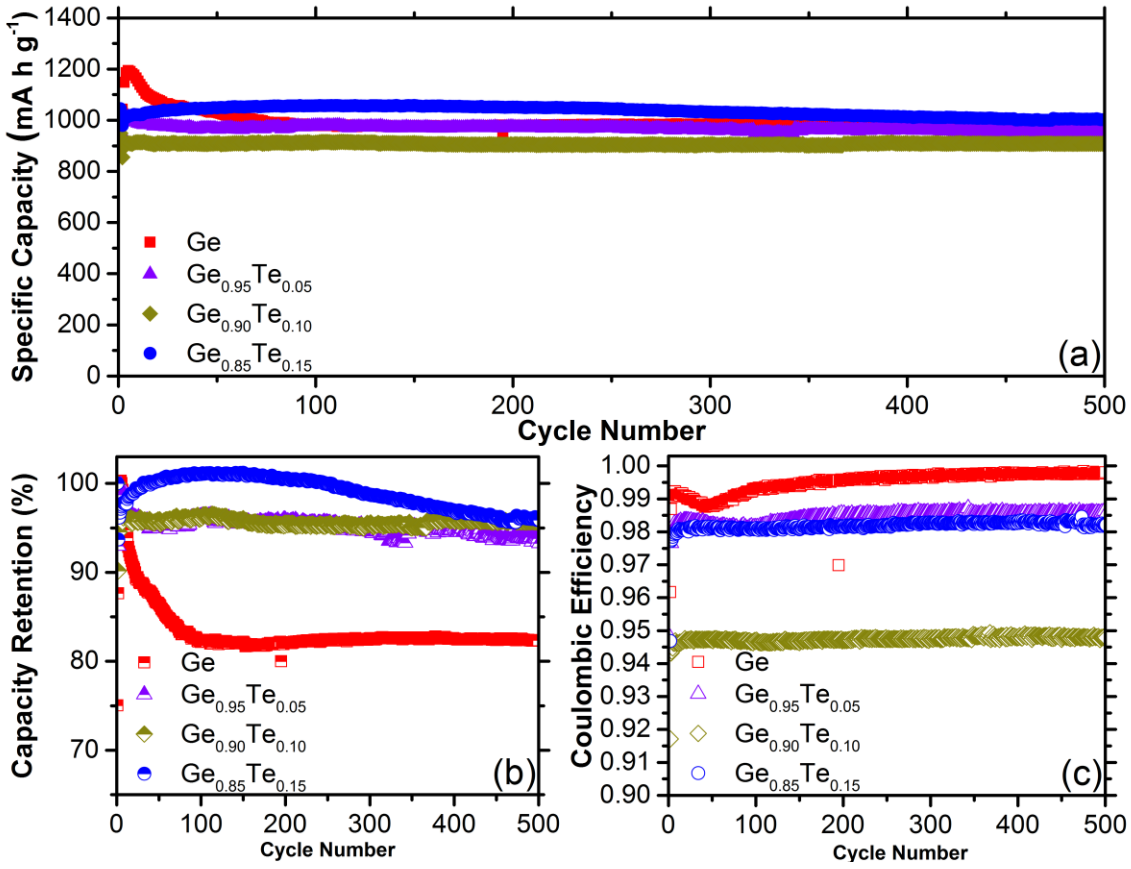

Figure 9. (a) Specific capacity, (b) capacity retention, and (c) coulombic efficiency for Ge (red), $Ge_{0.95}Te_{0.05}$ (purple), $Ge_{0.90}Te_{0.10}$ (green), $Ge_{0.85}Te_{0.15}$ (blue) after 500 cycles at a rate of 1C.

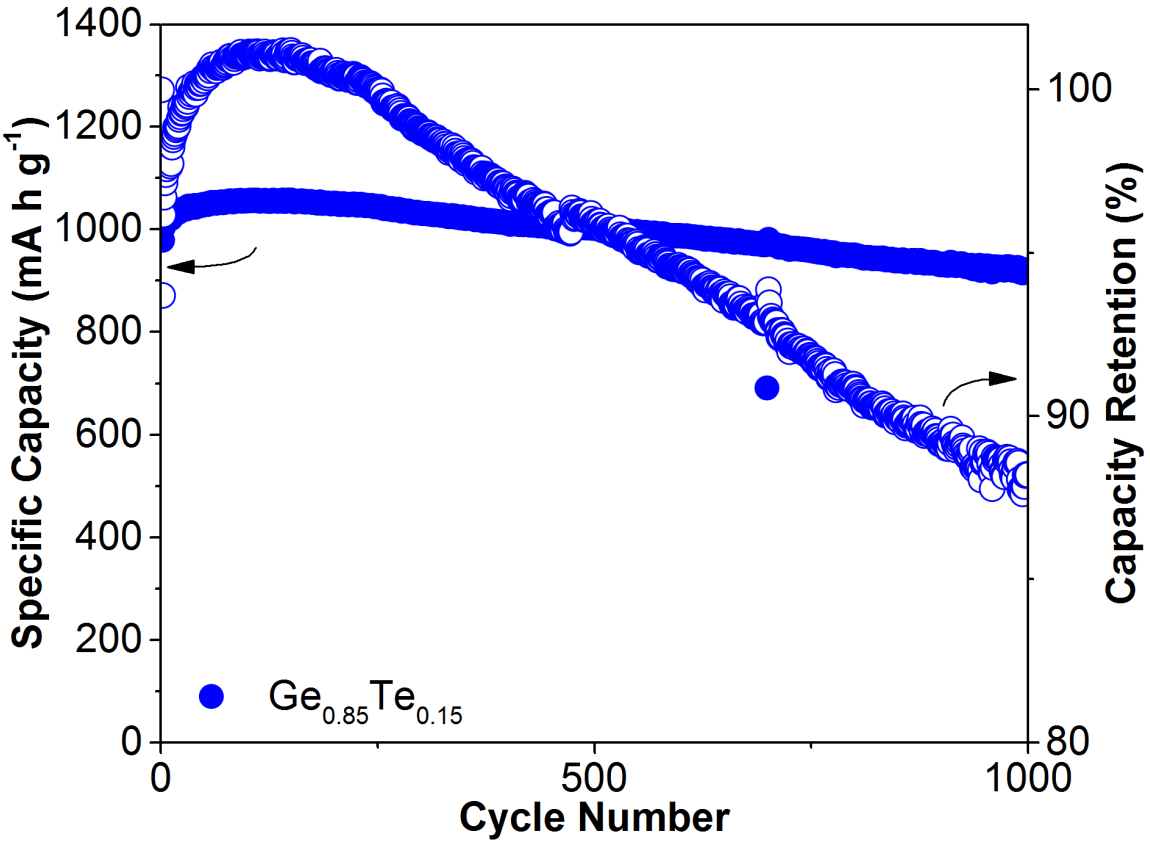

Figure 10. Specific capacity and capacity retention for $Ge_{0.85}Te_{0.15}$ after 1000 cycles at 1C.

To visualize the chemical reactions occurring in each cycle, information from the cycling data can be extracted to make a voltage-capacity plot. Voltage-capacity plots for cycling at a rate of 1C are shown for Ge, $Ge_{0.95}Te_{0.05}$, $Ge_{0.90}Te_{0.10}$, and $Ge_{0.85}Te_{0.15}$ in Figure 11. The discharge (lithium insertion) cycles are represented with solid lines and the charge (lithium extraction) cycles are represented with dashed lines. Cycles 1, 50, 100, and 500 are compared for each material. The area under the curve for cycle 1 between 1.50V vs. Li/Li^+ to 0.75V vs. Li/Li^+ increases as the amount of tellurium in the germanium is increased. This area under the curve is much larger in $Ge_{0.85}Te_{0.15}$ than Ge. This is attributed to the formation of the Li_2Te phase and its additional contribution to

capacity. We anticipate that 15 atomic % Te in the $Ge_{0.85}Te_{0.15}$ material will only contribute about 80 mAh g^{-1} to the initial capacity in cycle 1. The area under the cycle 1 curve in $Ge_{0.85}Te_{0.15}$ accounts for about 180 mAh g^{-1}, we attribute the extra 100 mAh g^{-1} of capacity to the formation of the solid-electrolyte interphase layer.

The voltage-capacity plots also indicate the stability of the cycling material. This can be determined by looking at the overlap of the charge and discharge curves for different cycles. In the Ge material the discharge and charge lines do not overlap for any of the cycles. This indicates that the material is losing capacity as the cycle number is increasing. In contrast, in the $Ge_{0.85}Te_{0.15}$ material the discharge and charge lines overlap almost exactly for cycles 50 and 100. This indicates that the material is not losing capacity over these cycles. The line for cycle 500 is only slightly lower in capacity than cycles 50 and 100, which suggest the material is stable.

The charge and discharge lines for $Ge_{0.95}Te_{0.05}$ overlap to a lesser degree than those for $Ge_{0.85}Te_{0.15}$ which indicates that it cycles with less stability. The charge and discharge lines for $Ge_{0.90}Te_{0.10}$ have more overlap than $Ge_{0.95}Te_{0.05}$ but they have less overall capacity than $Ge_{0.85}Te_{0.15}$.

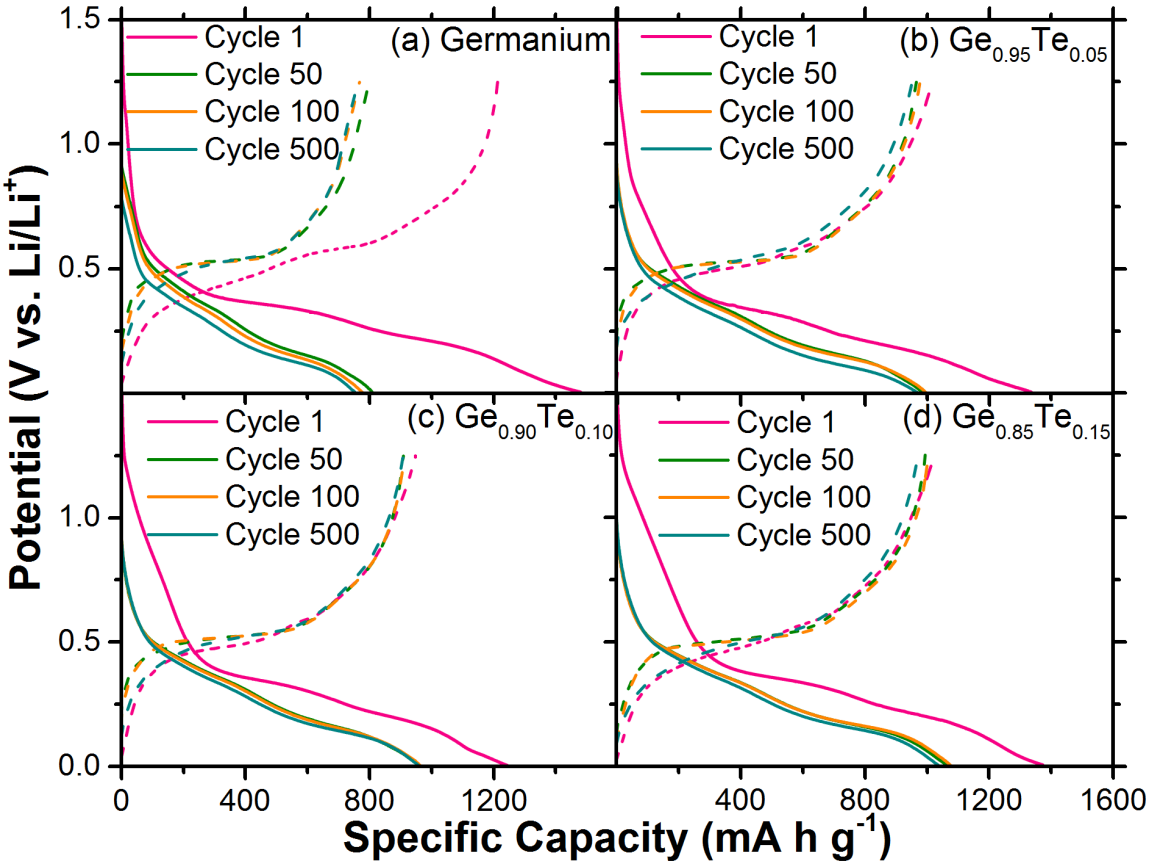

Figure 11. Voltage-capacity profiles of cycles 1, 50, 100, and 500 for (a) Ge, (b) $Ge_{0.95}Te_{0.05}$, (c) $Ge_{0.90}Te_{0.10}$, and (d) $Ge_{0.85}Te_{0.15}$.

The plateaus that occur in the voltage-capacity plots indicate the potential at which new phases of material are formed. The pseudo-plateaus at about 0.45V and 0.3V vs. Li/Li^+ correspond to the formation of Li-Ge alloys.[32] Taking the derivative of the specific capacity with respect to voltage, and plotting this versus potential gives a differential capacity plot. These plots have peaks that correspond to the formation of new phases. Peaks make it easy to identify at which potential a phase is forming. The differential capacity plots indicate that new phases are being formed as lithium is being inserted and extracted. These plots are very similar to cyclic voltammograms. Figures 12, 13, and 14, below show the differential-capacity plots of the $Ge_{(1-x)}Te_x$ materials for

cycles 2, 100, and 500, respectively. The data for these plots was extracted from the 1C cycling data reported in Figures 9 and 10 above.

The sharpness of the peaks gives information about the crystallinity or amorphousness of the material. A thin, sharp peak indicates the phase is a crystalline material. A broad peak indicates that the phase is amorphous.[33-35] Figure 12 shows the differential capacity curves for Ge (red), $Ge_{0.95}Te_{0.05}$ (purple), $Ge_{0.90}Te_{0.10}$ (green), and $Ge_{0.85}Te_{0.15}$ (blue) at cycle 2. For the lithium extraction curves (positive dQ/dV values) at ~0.6V vs. Li/Li^+ the peak looks different for the different materials. The peak is less broad and sharper for Ge and $Ge_{0.95}Te_{0.05}$, while it is broader and less sharp for $Ge_{0.90}Te_{0.10}$ and $Ge_{0.85}Te_{0.15}$. This indicates that Ge and $Ge_{0.95}Te_{0.05}$ are more crystalline than $Ge_{0.90}Te_{0.10}$ and $Ge_{0.85}Te_{0.15}$.

This theme is repeated in Figure 13, which shows the differential capacity plots of $Ge_{(1-x)}Te_x$ materials at cycle 100 after cycling at a rate of 1C. In this plot, Ge, $Ge_{0.95}Te_{0.05}$, and $Ge_{0.90}Te_{0.10}$ are more crystalline than $Ge_{0.85}Te_{0.15}$. This is demonstrated because Ge, $Ge_{0.95}Te_{0.05}$, $Ge_{0.90}Te_{0.10}$ have sharper peaks than $Ge_{0.85}Te_{0.15}$.

In Figure 14, $Ge_{0.85}Te_{0.15}$ continues to be amorphous, as demonstrated by the short, broad lithium extraction peak. However, $Ge_{0.95}Te_{0.05}$ also becomes more amorphous than Ge and $Ge_{0.90}Te_{0.10}$. Overall, the amorphousness of the $Ge_{0.85}Te_{0.15}$ material may contribute to the cycling stability of the material at a rate of 1C.

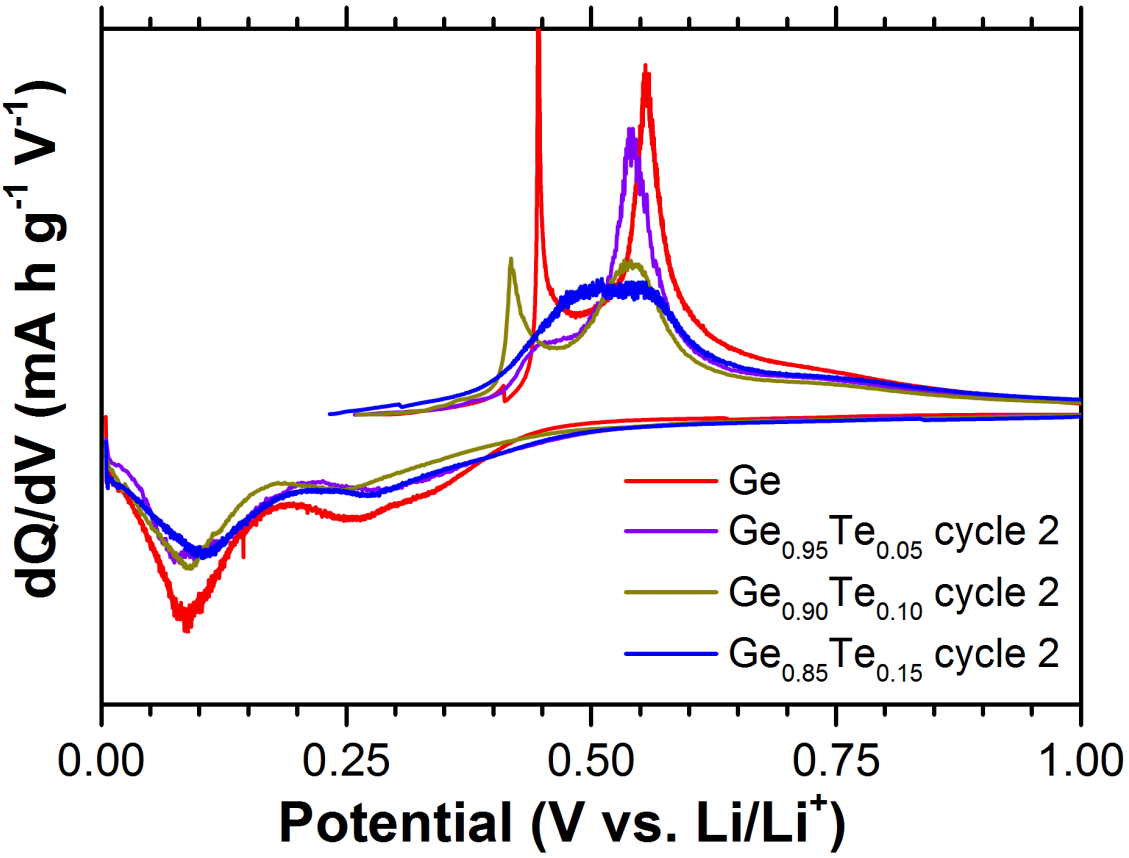

Figure 12. Differential capacity plots of Ge (red), $Ge_{0.95}Te_{0.05}$ (purple), $Ge_{0.90}Te_{0.10}$ (green), $Ge_{0.85}Te_{0.15}$ (blue) after cycle 2 of 1C cycling.

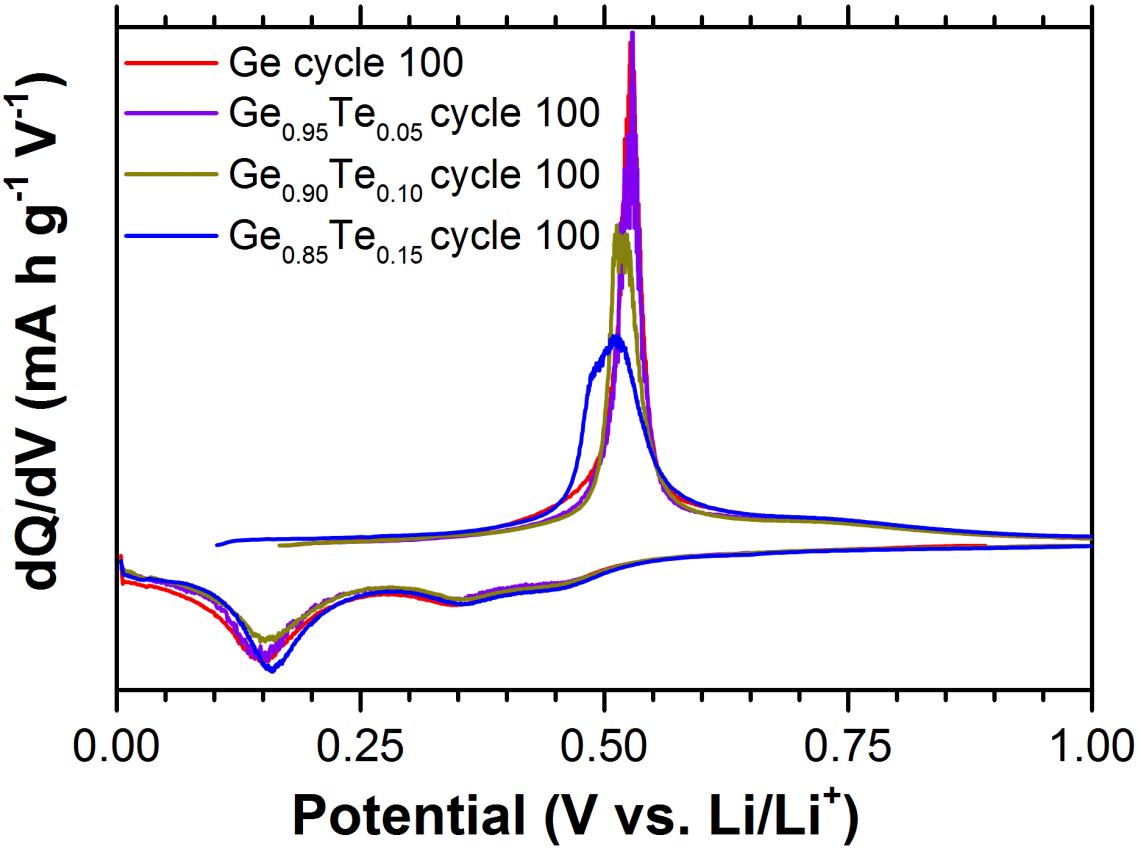

Figure 13. Differential capacity plots of Ge (red), $Ge_{0.95}Te_{0.05}$ (purple), $Ge_{0.90}Te_{0.10}$ (green), $Ge_{0.85}Te_{0.15}$ (blue) after cycle 100 of 1C cycling.

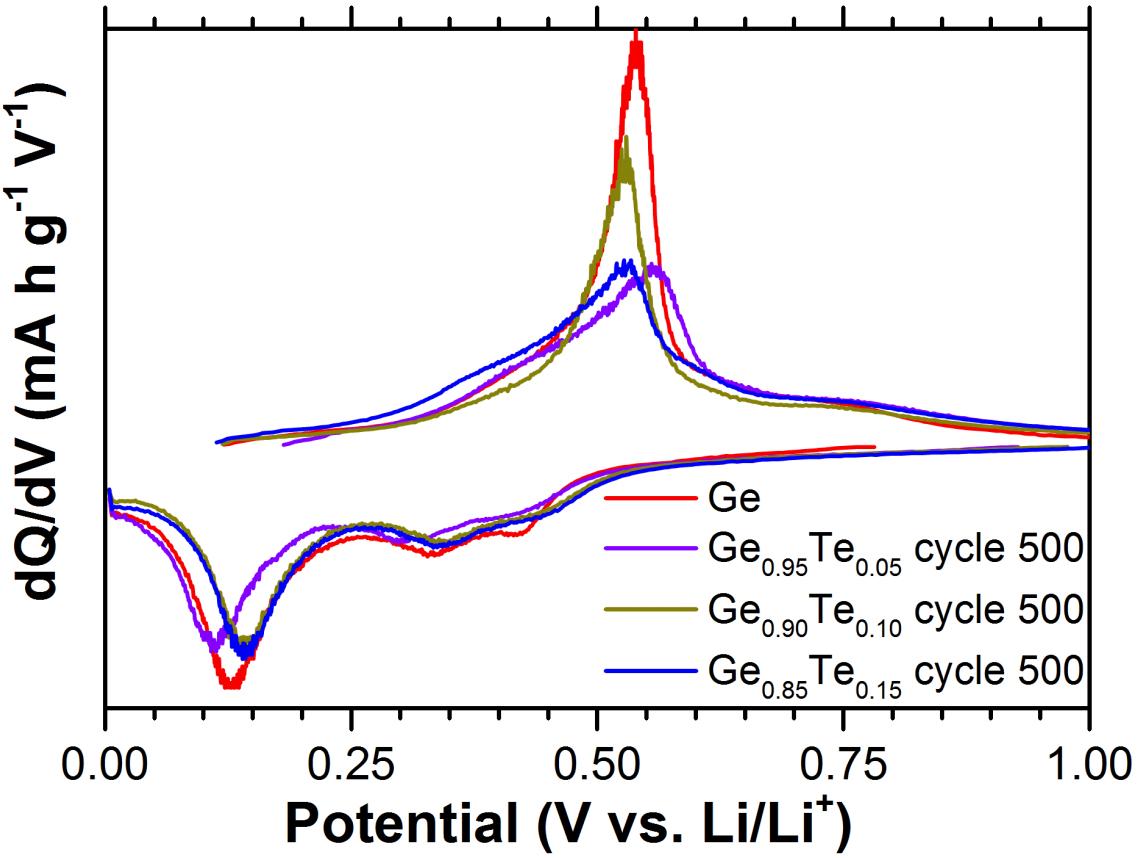

Figure 14. Differential capacity plots of Ge (red), $Ge_{0.95}Te_{0.05}$ (purple), $Ge_{0.90}Te_{0.10}$ (green), $Ge_{0.85}Te_{0.15}$ (blue) after cycle 500 of 1C cycling.

AC impedance spectra were obtained of the Ge and $Ge_{0.85}Te_{0.15}$ electrodes at open circuit potentials after at least 500 cycles at a rate of 1C and de-lithiated to 1.25V vs. Li/Li^+, Figure 15. The frequency range was 0.01 Hz to 100k Hz with a perturbing voltage of 5 mV vs. Li/Li^+.

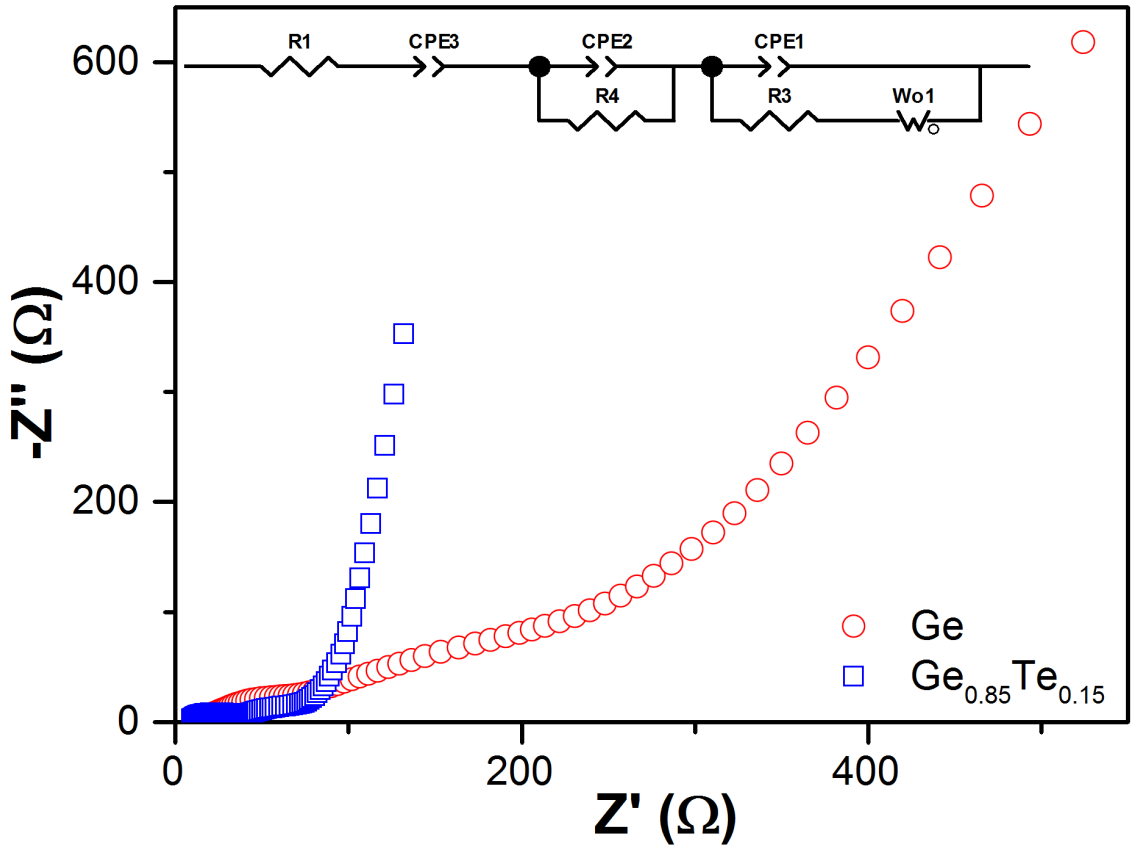

Figure 15. Impedance spectra (Nyquist plots) of the Ge and $Ge_{0.85}Te_{0.15}$ electrodes de-lithiated to 1.25 V vs. Li/Li^+ after at least 500 cycles. The equivalent circuit is shown in the inset. Frequency range 100k Hz to 0.01 Hz, 5 mV vs. Li/Li^+ perturbing voltage.

The Warburg impedance term derived of the impedance spectrum of Figure 15 indicates that Li^+-diffusion in the $Ge_{0.85}Te_{0.15}$ electrode is about three times faster than in the germanium electrode. This suggests that the better cycling performance of the $Ge_{0.85}Te_{0.15}$ electrode derives from the presence of the non-cycling Li_2Te phase, which maintains the lithium alloys of Ge in an amorphous state.

CONCLUSIONS

A series of micrometer-sized particles of novel germanium sub-telluride materials and micrometer-sized particles of pure germanium were synthesized using melt-quench and high intensity ball milling techniques. It was shown that tellurium was successfully incorporated into the germanium active material, and upon cycling an inactive Li_2Te phase was formed. The materials were compared using electrochemical cycling versus lithium metal. Phases formed upon reaction with lithium were analyzed using cyclic voltammetry, voltage-capacity plots, and differential capacity plots. The cycling performances of all $Ge_{(1-x)}Te_x$ materials were compared at rates of C/5 and 1C. It was determined that $Ge_{0.85}Te_{0.15}$ exhibited the highest capacity and best cycling stability. The formation of the Li_2Te phase and the amorphousness of $Ge_{0.85}Te_{0.15}$ upon cycling contributed to the improved cycling stability of $Ge_{0.85}Te_{0.15}$ over Ge.

References

1. S. Han, J. Park, W. Lu and A. M. Sastry, *Journal of Power Sources*, 2013, **240**, 155-167.
2. Y. R. Kolobov, G. P. Grabovetskaya, M. B. Ivanov, A. P. Zhilyaev and R. Z. Valiev, *Scripta Materialia*, 2001, **44**, 873-878.
3. J. Horvath, R. Birringer and H. Gleiter, *Solid State Communications*, 1987, **62**, 319-322.
4. T. Mutschele and R. Kirchheim, *Scripta Metallurgica* 1987, **21**, 135-140.
5. D. Aurbach and O. Haik, in *Inorganic Nanoparticles: Synthesis, Applications, and Perspectives*, eds. C. Altavilla and E. Ciliberto, CRC Press, Boca Raton, 2011, vol. 2, ch. 9, pp. 213-256.
6. J. Graetz, C. C. Ahn, R. Yazami and B. Fultz, *Journal of the Electrochemical Society*, 2004, **151**, A698.
7. C. S. Fuller and J. C. Severiens, *Physical Review*, 1954, **96**, 21-24.
8. R. Amatya and R. J. Ram, *Journal of Electronic Materials*, 2011, **41**, 1011-1019.
9. J. Sangster, *Journal of Phase Equilibria*, 1997, **18**, 289-294.
10. L. Baggetto and P. H. L. Notten, *Journal of the Electrochemical Society*, 2009, **156**, A169.
11. L. Y. Lim, N. Liu, Y. Cui and M. F. Toney, *Chemistry of Materials*, 2014, **26**, 3739-3746.
12. A. N. Dey, *Journal of the Electrochemical Society*, 1971, **118**, 1547-1549.
13. A. M. Chockla, K. C. Klavetter, C. B. Mullins and B. A. Korgel, *ACS Applied Materials &Iinterfaces*, 2012, **4**, 4658-4664.
14. C. K. Chan, X. F. Zhang and Y. Cui, *Nano Letters*, 2008, **8**, 307-309.
15. H. Lee, M. G. Kim, C. H. Choi, Y. K. Sun, C. S. Yoon and J. Cho, *Journal of Physical Chemistry B*, 2005, **109**, 20719-20723
16. Y. Kim, H. Hwang, K. Lawler, S. W. Martin and J. Cho, *Electrochimica Acta*, 2008, **53**, 5058-5064.
17. Y.-M. Lin, K. C. Klavetter, A. Heller and C. B. Mullins, *The Journal of Physical Chemistry Letters*, 2013, **4**, 999-1004.
18. Y. J. Cho, H. S. Im, Y. Myung, C. H. Kim, H. S. Kim, S. H. Back, Y. R. Lim, C. S. Jung, D. M. Jang, J. Park, E. H. Cha, S. H. Choo, M. S. Song and W. I. Cho, *Chemical Communications*, 2013, **49**, 4661-4663.
19. P. R. Abel, K. C. Klavetter, K. Jarvis, A. Heller and C. B. Mullins, *Journal of Materials Chemistry A*, 2014, **2**, 19011-19018.
20. P. R. Abel, K. C. Klavetter, A. Heller and C. B. Mullins, *The Journal of Physical Chemistry C*, 2014, **118**, 17407-17412.
21. K. C. Klavetter, J. P. de Souza, A. Heller and C. B. Mullins, *Journal of Materials Chemistry A*, 2015, **3**, 5829-5834.
22. H. X. Dang, K. C. Klavetter, A. Heller and C. B. Mullins, *Journal of Materials Chemistry A*, 2015, **3**, 13500-13506.

23. S. M. Wood, K. C. Klavetter, A. Heller and C. B. Mullins, *Journal of Materials Chemistry A*, 2014, **2**, 7238.
24. Y. Liu, J. Wang, Y. Xu, Y. Zhu, D. Bigio and C. Wang, *Journal of Materials Chemistry A*, 2014, **2**, 12201.
25. J. Zhang, Y.-X. Yin, Y. You, Y. Yan and Y.-G. Guo, *Energy Technology*, 2014, **2**, 757-762.
26. S. Chakraborty and P. Boolchand, *Journal of Physical Chemistry B*, 2014, **118**, 2249-2263.
27. MDI Software. JADE. http://www.materialsdata.com/.
28. *Constitution of binary alloys*, McGraw-Hill, New York, 1958.
29. E. Carria, A. M. Mio, S. Gibilisco, M. Miritello, C. Bongiorno, M. G. Grimaldi and E. Rimini, *Journal of the Electrochemical Society*, 2012, **159**, H130.
30. J. G. Fleming and D. A. Stevenson, *Journal of the Electrochemical Society*, 1989, **136**, 3859-3863.
31. B. Laforge, L. Levan-Jodin, R. Salot and A. Billard, *Journal of the Electrochemical Society*, 2008, **155**, A181.
32. M. R. St. John, A. J. Furgala and A. F. Sammells, *Journal of the Electrochemical Society: Electrochemical Science and Technology*, 1982, **129**, 246-250.
33. R. A. Huggins, *Ionics*, 1997, **3**.
34. R. A. Huggins, *Solid State Ionics*, 1998, **113-115**, 57-67.
35. R. A. Huggins, *Journal of Power Sources*, 1999, **81-82**, 13-19.